STARK EFFECT IN COLLOIDAL PBS NANOSHEETS

Kiran Lamichhane

A Thesis

Submitted to the Graduate College of Bowling Green
State University in partial fulfillment of
the requirements for the degree of

MASTER OF SCIENCE

August 2023

Committee:

Liangfeng Sun, Committee Chair

Marco Nardone

Alexey Zayak

ABSTRACT

Liangfeng Sun, Committee Chair

Due to their tunable energy gap and high quantum efficiency, lead sulfide (PbS) nanosheets exhibit high potential in photovoltaics and optoelectronics applications. Exciton dynamics play a vital role in the performance of the devices based on this material. We measured the time-resolved photoluminescence spectra of PbS nanosheets to study the dynamics of the excitons in PbS nanosheets. The photoluminescence peak of the nanosheets shifts to longer wavelengths in a few hundred nanoseconds time window after excitation by a picosecond pulsed laser.

The Stark effect leads to the redshift of the photoluminescence spectrum of the PbS nanosheets. The dangling bonds of the surface sulfur atoms lead to a static electric field which reduces the energy gap of the nanosheet – so called Stark effect. Under pulsed laser excitation, the photoexcited charge carriers (excitons) screen the static electric field, reducing the Stark effect. Consequently, a blue-shifted photoluminescence peak, corresponding to a larger band gap, is observed. The carrier recombination resumes the Stark effect, leading to a red shift of the photoluminescence peak. Since the surface states, either charged or polarized, attract the excitons to them before they undergo recombination, the time-dependent photoluminescence spectrum reveals the exciton diffusion process in the 2D nanosheets. The control experiment using quantum dots, however, does not show such time-dependent red shift of the photoluminescence spectrum. The absence of the red shift is due to the small size of the quantum dots where no excess excitons exist to reduce the Stark effect.

I dedicate this thesis to my parents, sister, and wife.

ACKNOWLEDGMENTS

I want to express sincere gratitude to my advisor Dr. Liangfeng Sun for giving me the opportunity to work under his supervision. I am immensely thankful for his guidance, expertise, and unwavering support. I am so grateful for his invaluable insights, constructive feedback, and continuous encouragement. I know that his support will be invaluable as I move forward. I am also grateful to my thesis committee members, Dr. Marco Nardone and Dr. Alexey Zayak, for their thoughtful comments and suggestions on my work. I would like to extend my thanks to all my research group members for their support. I want to express my appreciation to the Department of Physics and Astronomy for their support in completing my research. Finally, I acknowledge that this material is based upon work supported by the National Science Foundation under Grant No. [1905217].

TABLE OF CONTENTS

Page

LIST OF FIGURES

LIST OF TABLES

CHAPTER 1. INTRODUCTION

1.1 Quantum Confinement and Nanomaterials

The development of science and technology in the past few years has allowed scientists to manipulate materials at the atomic and molecular levels leading to the advancement of nanotechnology. Nanotechnology is emerging as a new and relevant sector with the potential for revolutionizing a broad range of fields, from electronics[1, 2] and medicine[3-6] to environmental sciences[7, 8] and agriculture[9, 10]. Nanotechnology refers to engineering materials on a scale of 1 nm to 100 nm and exploring their properties for various applications. The development of nanotechnology has brought advancements that were unimaginable a few decades ago. Nanomaterials' unique properties result from the phenomenon called the quantum confinement effect, which refers to the change in the behavior of materials when confined to nanoscale dimensions.

Quantum confinement refers to the profound effect of size reduction on the electronic and optical properties of the materials[11-13]. Reducing the size of materials from bulk to nanoscale dimensions shows a notable increase in the energy band gap and the nature of energy bands. In bulk materials, the energy bands are overlapped, allowing for the flow of electrons. However, when the size of the material becomes comparable to the exciton Bohr radius, the continuous energy levels of the bulk materials transform into discrete energy levels[14, 15]. The exciton Bohr radius is a critical limit determined by the materials' lattice structure and dielectric property[16, 17]. We can calculate the exciton Bohr radius using the following formula[16].

$$a_0 = \frac{4\pi\varepsilon\hbar^2}{m^* q^2}$$

In this equation, ε is the dielectric constant of the material, $\hbar$ is the reduced Plank's constant, m^* is reduced effective mass of the electron and hole, and q is a charge of an electron.

Exciton Bohr radii of general semiconductor range from 0.7 nm for CuCl[18] to 65.6 nm for InSb[19]. The materials of our interest have Bohr radii of 20 nm for PbS, 46 nm for both PbSe and 104 nm for PbTe[20, 21].

As the size of the nanomaterial decreases further, the confinement effect becomes more pronounced. Nanomaterials are classified as zero-dimensional (0-D), one-dimensional (1-D), and two-dimensional (2-D) materials based on the directions of confinement. 0-D materials are confined in all three directions, 1-D materials are confined in two directions, and 2-D materials are confined in one direction. The direction of confinement restricts the electrons from moving in that specific direction. Figure 1 represents the density of states (DOS) for different structural dimensions of the material[22].

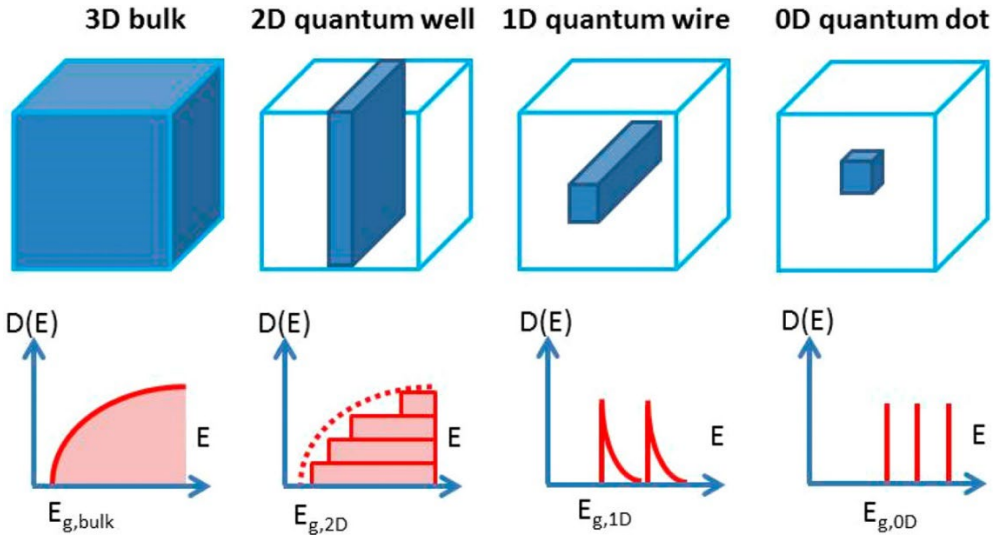

Figure 1. Schematic representation of the density of states of bulk, 1-D confined, 2-D confined, and 3-D confined materials from left to right.

0-D, 1-D, and 2-D nanomaterials are named quantum dots (QDs), nanorods/nanowires (NWs), and nanosheets (NSs), respectively. This classification system provides a framework for understanding nanomaterials' varying degrees of confinement and helps illustrate their unique

properties. The effective band gap of 3-D confined quantum dots is given by the following equation[23].

$$E_{eff} \cong E_g + \frac{\hbar^2 \pi^2}{2R^2}\left(\frac{1}{m_e} + \frac{1}{m_h}\right) - \frac{1.8e^2}{\epsilon R}$$

In this equation, E_g is the band gap of bulk form, R is the radius of the quantum dot, m_e and m_h are the effective mass of the electron and hole, respectively, and ϵ is the dielectric constant of the semiconductor. The second term on the right represents the confinement energy, and the last term is the Coulomb interaction. The radius of the quantum dot contributes to an increase in the band gap due to confinement and a decrease in the band gap due to Coulomb interaction. But the contribution in confinement is higher than the Coulomb interaction.

1.2 Objective of This project

The unique and versatile properties of nanomaterials because of the quantum confinement effect led to the possibilities of a vast range of applications. Several processes are developed to make typical quantum-confined structures. Chemical vapor deposition (CVD) and Molecular beam epitaxy (MBE) are the popular methods for making thin films. The solution methods are gaining more popularity as these methods are significantly cheaper despite the process being dirty and difficult to characterize. The colloidal synthesis process involves mixing precursors at high temperatures, and the reaction contains ligands that are attached to the particles' surface, which keep them from aggregation[24] and provide an oleophilic surface for solubility. The size of quantum dots can be tuned, varying the reaction temperature and the amount of ligands in the solution [25].

Most colloidal quantum dots are binary compound semiconductors combining III-V, II-VI, and IV-VI groups' elements forming the quantum dots[25, 26] of size 2-10 nm. Our interest and work are on lead sulfide (PbS), an IV-VI combination. PbS has a rock-salt crystal structure with

a lattice constant of 5.934 A^{o}. The bulk PbS has an energy band gap of 0.41 eV[27]. PbS quantum dots have a tunable energy gap from 0.6 eV to 1.8 eV [26, 28], covering the energy range around the near-infrared (NIR) region. Since PbS has an exciton Bohr radius of 20 nm, it is easier to make its quantum-confined structures. They also have a higher quantum yield (QY) in NIR wavelengths than organic fluorophores [29-31].

Exploring static and temporal photoluminescence and studying the exciton decay dynamics of colloidal lead sulfide (PbS) nanosheets is the goal of this project. A tunable energy band, large carrier mobility, and good absorbance make PbS a suitable candidate for optoelectronic and photovoltaic applications. Therefore, we studied the photoluminescence (PL) decay dynamics to investigate the dynamics of excited states in PbS nanomaterials which is important for applicational purposes.

1.3 PbS Quantum Dots Versus Nanosheets

Recent research has shown that nanosheets are becoming increasingly popular due to their advantages over quantum dots. Unlike quantum dots, nanosheets have better mobility of electrons in their lateral direction because the surface ligands in quantum dots act as an obstacle for charge transport[32], as shown in Figure 2[33]. Additionally, quantum dots have a hindrance to their efficiency due to non-radiative Auger recombination caused by strong exciton-exciton interaction. This problem is reduced in PbS nanosheets because their broader lateral dimensions provide more space for excitons, which decreases their interaction with each other[33]. Therefore, nanosheets are emerging as solutions to the shortcomings of quantum dots preserving their confinement properties[32, 34-37].

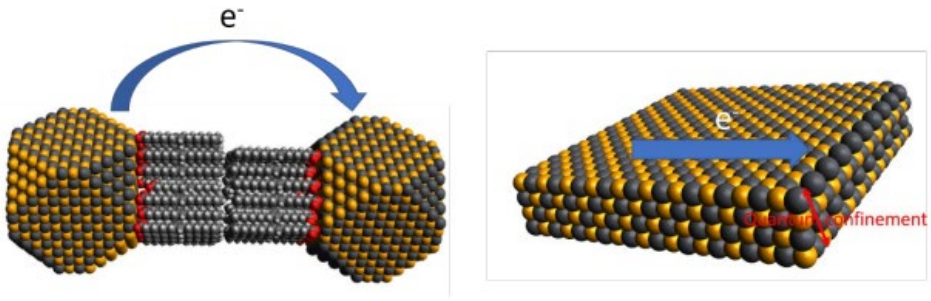

Figure 2. Electrons mobility schemes between quantum dots and within a nanosheet.

The synthesis of PbS nanosheets involves the two-dimensional oriented attachment of PbS quantum dots[32], facilitated by chloroalkane. The thickness of nanosheets is tuned by changing the reaction temperature[35] and growth time[38]. PbS nanosheets have an emission range that varies from 720 nm to 2100 nm depending on their lateral size and thickness[32, 34-36, 39, 40]. The lateral widths of PbS nanosheets affect their performance as narrower nanosheets have higher quantum yields (QY) than broader ones due to the presence of fewer surface states[39].

1.4 Excitons and Stark Effect in Colloidal PbS Nanoribbons

Exciton is a quasiparticle that forms when a material absorbs a photon. Each semiconductor possesses its unique energy band gap, which is the separation between valence band and conduction band. When a material is hit by a beam of light, the electrons get excited and jump from the valence band to the conduction band, leaving positively charged holes in the valence band, as shown in Figure 3. This electron-hole pair is known as exciton and are bounded together by the Coulomb force. The behavior of excitons is impacted by the dimensionality, morphology, and presence of trap states in the nanomaterials. Exciton can deactivate through various channels. They can undergo radiative recombination, where energy is released as a photon, or non-radiative recombination, where energy is dissipated through phonons or defects. Radiative recombination occurs by emitting a photon with an energy equal to the band gap. This

process is crucial for optoelectronic devices and photovoltaic applications, where the efficient conversion of excitonic energy into light is required.

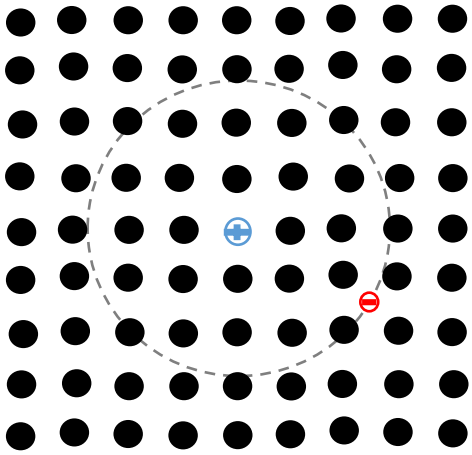

Figure 3. Exciton; a bound state due to Coulomb attraction between a hole and an electron excited by absorbing a photon.

In this project, we compared exciton decay dynamics in PbS quantum dots and PbS nanoribbons within a few hundred nanoseconds after exciting the sample using a pulsed laser. We see the red shift in the PL spectrum of delayed emission and confirm that the surface trap states are responsible for the shift. The presence of surface defects in nanoribbons results in building an electric field, which interacts with excited states shifting the original energy levels, and the phenomenon is called the Stark effect. The Stark effect is the shifting and splitting of spectral lines in the presence of an external electric field.

We also studied the effect of excitation intensity on the PL spectrum. As the intensity increases, multiple excitons are generated in the nanosheets, creating an inbuilt electric field. This electric field causes a change in the PL spectrum, which we observed during the experiment. We noted a blue shift in the PL emission as excitation power increased, which can be attributed to the screening of the Stark effect resulting from the inbuilt electric field by the excited electrons.

CHAPTER 2. EXPERIMENTAL METHODS

2.1 Synthesis Setup

We used a standard Schlenk line system setup, as shown in Figure 4[41], inside the fume hood for all the synthesis. The Schlenk line system is designed to supply nitrogen or provide a vacuum and create air-free conditions to prevent the reaction from atmospheric contamination. The Schlenk line system consists of two parallel glass tubes called a dual manifold, which is the central body part of the system. One tube is connected to the nitrogen supply and the oil bubbler. The oil bubbler provides pressure to the nitrogen supply, which helps to observe the rate of nitrogen flow in the system. The other tube is connected to the vacuum pump via a cold trap. The cold trap is submerged in Dewar with liquid nitrogen, which stops harmful solvents from entering the pump. Those solvents from the reaction can damage the pump oil and the pump.

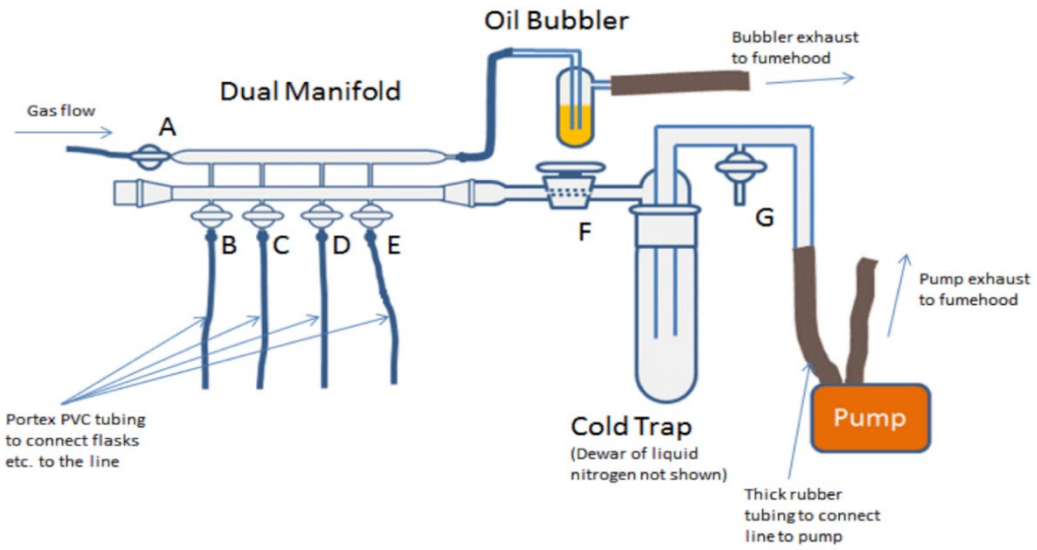

Figure 4. Schematic diagram of Schlenk line system.

2.1.1 Synthesis of PbS Nanoribbons

The synthesis of colloidal PbS nanoribbon is adapted from a method developed by Sun's group[39]. The lead precursor is prepared by dissolving 506 mg lead oxide in 10 ml diphenyl ether and 1.8 ml oleic acid in a 3-necked flask at 110°C for 1 hour. Then the mixture is over-degassed

for 20 minutes at 100ºC. After degassing, 1 ml of 1,1,2-trichloroethane is added at 110ºC, and allow the reaction to complete for 30 minutes. The sulfur precursor is prepared by dissolving 12 mg thioacetamide in 70 µl dimethylformamide and 930 µl trioctylphosphine in a nitrogen environment in another 3-necked flask. The sulfur precursor is then injected into the flask with lead precursor set at the desired temperature (70ºC to 130ºC), as shown in Figure 5, and the reaction time is set accordingly. After completing the reaction, the solution is let alone to cool down, reaching room temperature. The final product is washed with toluene two times and precipitated using a centrifuge. Finally, the precipitated nanoribbons are re-dispersed and stored in toluene.

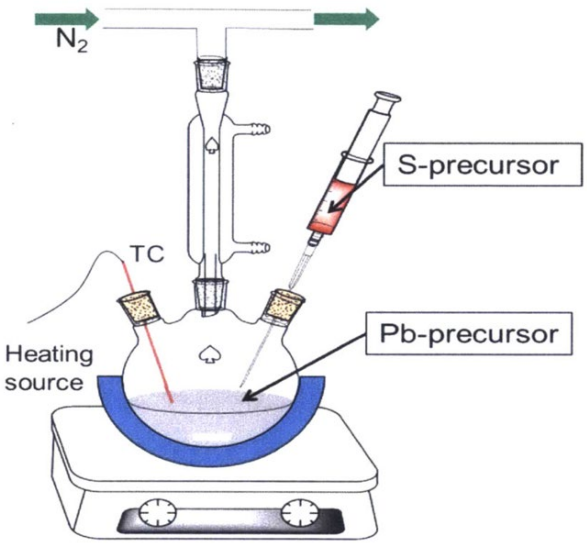

Figure 5. Experimental setup for the synthesis of PbS nanosheets[42].

2.1.2 Synthesis of PbS Quantum Dots

The synthesis of colloidal PbS quantum dots is in the identical setup to the synthesis of nanoribbons, and the recipe for the synthesis is adopted from Hines's group method[26]. In this process, the lead precursor is prepared by dissolving 220 mg lead oxide in 5 ml Oleic acid and 5 ml 1-octadecene (varying the amount of Oleic acid and 1-octadecane so that the total volume is 10 ml leads to the formation of different sizes of quantum dots) using a magnetic stir bar in a 3-

necked flask at 150ºC for 1 hour. The reaction is sealed using a rubber septum and heated in a nitrogen environment. Then the mixture is degassed for 20 minutes at 100ºC. The sulfur precursor is prepared by mixing 6 ml 1-octadecane and 126 µl hexamethyldisilathiane in another 3-necked flask with a magnetic stir bar under a nitrogen environment for 30 minutes. The sulfur precursor is then injected into the flask with lead precursor set at the desired temperature (90ºC to 150ºC). The mixture can complete the reaction in 1 minute and is immediately cooled using an ice bath. All the processes are performed under the nitrogen environment. The final product is washed with methanol and butanol two times and precipitated using a centrifuge. Finally, the precipitated quantum dots are re-dispersed and stored in hexane.

2.2 Photoluminescence (PL) Spectroscopy

Photoluminescence (PL) spectroscopy studies light emission from a material after it absorbs photons. It is a non-destructive method in which the sample is hit with a laser or intense light. The sample absorbs photons, and electrons jump from lower or ground states to higher energy states. Electrons cannot stay in those higher energy or excited states forever, known as metastable states. Therefore, the excited electrons relax back to the ground states emitting photons. By studying the emission spectrum, we can extract information about the band gap, energy levels, defects, purity, etc. Figure 6[43] shows the general PL emissions processes.

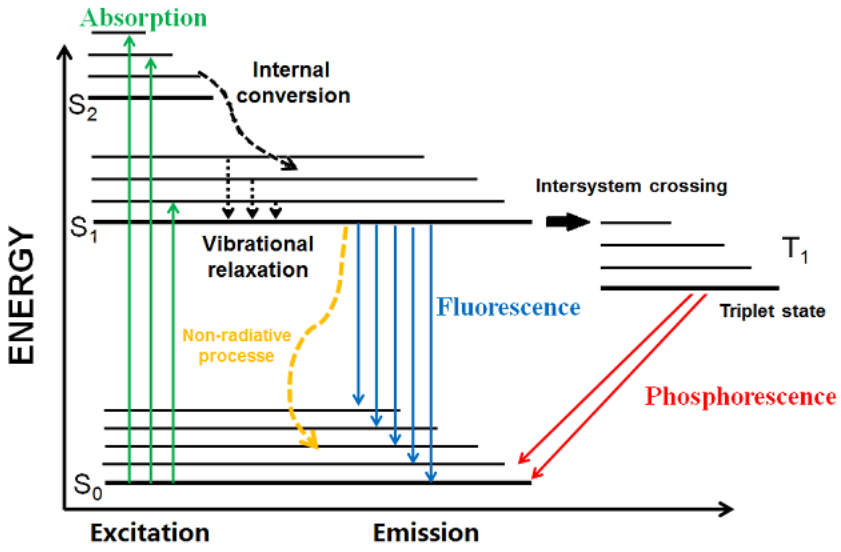

Figure 6. Schematic diagram of Fluorescence and Phosphorescence demonstrating the processes of excitation of electrons by absorbing energy and recombination through radiative and non-radiative channels.

The emitted photon is red-shifted compared to the absorbed photon in PL emission. The reason is that incident photon energy dissipation occurs through different relaxation processes like vibrational relaxation and non-radiative recombination other than fluorescence and phosphorescence.

A home-built spectrometer system, as shown in Figure 7, is used to measure PL emission. The system consists of an argon laser, a monochromator, and an infrared detector. Other than that, two reflecting mirrors and two irises are used to align the laser beam. A system of ND (Neutral Density) filters is used to tune the intensity of the laser, and a chopper is used to modulate the continuous laser into a pulsed one. Finally, two convex lenses collect the emitted photons from the sample into the detector. A long pass filter is placed at the entrance of the detector to cut off the laser signal. The sample is separated from the toluene and dispersed in tetrachloroethene for the PL measurement to avoid absorption by toluene. The colloidal solution is put in a quartz cuvette for the PL measurement. Figure 8 is the schematic diagram of the

spectrometer system to measure the PL emission. This system is run by software programmed in LabVIEW.

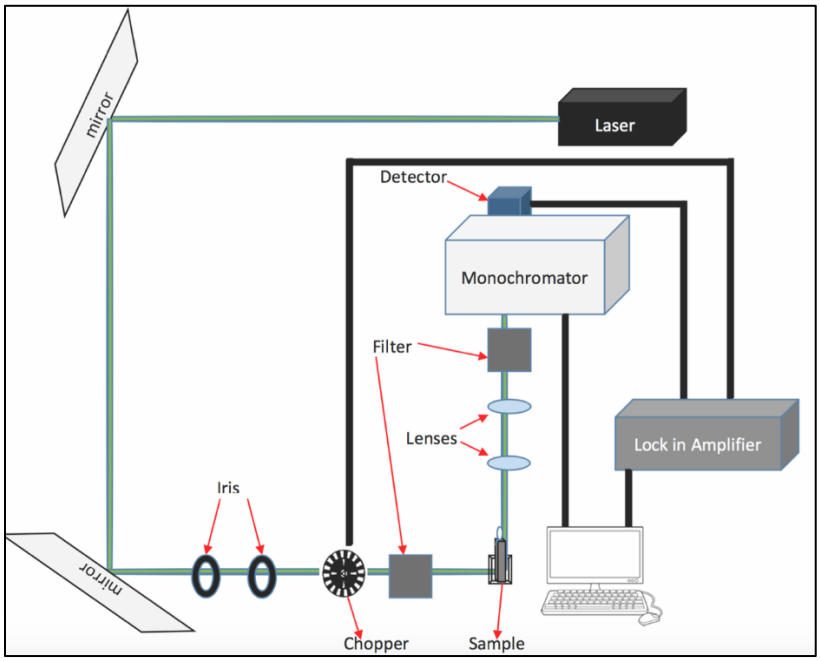

Figure 7. Schematic diagram of a system for measuring PL spectrum.

2.3 Time-Resolved Photoluminescence (TPL) Spectroscopy

Time-resolved photoluminescence (TPL) is measured using time-correlated single photon counting (TCSPC) system. An infrared pulsed laser (1064 nm) is a light source to excite the sample. The intensity of the laser is set between 0.1-0.8 watts and a frequency of 200 kHz for the measurement. Potassium titanyl phosphate (KTP) crystal generates a second harmonics of laser (532 nm) to excite the sample. A neutral density (ND) filter placed in the laser beam line tunes the intensity of the laser to avoid multiple excitons generation. And the photomultiplier tube (PMT) collects the emission signal into the TCSPC.

PL decay dynamics are studied using TPL spectroscopy and calculate the PL lifetime. Optically excited electrons in the conduction band relax back to the valence band, emitting

photons. The average time for an electron to return to the valence band after excitation is called PL lifetime. TCSPC system counts the photons emitted by relaxing electrons with time after excitation by a pulsed laser. The data of time against the emitted photon's intensity is fitted to the appropriate decay model to calculate the PL lifetime. In general, PL lifetime is the time to decrease the total intensity of emissions by factor 1/e or 37%. The total emission depends on the concentration of the sample, but the PL lifetime is independent of the concentration.

The PL lifetime of single exponential decay dynamics is calculated by fitting the data in the following equation.

$$I(t) = I_o e^{-\frac{t}{\tau}}$$

In this equation, *I(t)* is the intensity of emitted photons at time *t*, I_o is the intensity of emitted photons at time $t = 0$, and τ is the PL lifetime.

The PL lifetime of double exponential decay dynamics is calculated by fitting the PL decay using the following equation.

$$I(t) = A_1 e^{-\frac{t}{\tau_1}} + A_2 e^{-\frac{t}{\tau_2}}$$

In this equation, A_1 and A_2 are total fluorophores corresponding to lifetimes τ_1 and τ_2, respectively.

2.4 Time-Dependent PL Spectrum

We investigated the photoluminescence (PL) emission spectrum at various times after excitation. Our analysis was conducted through time-resolved photoluminescence (TPL) spectroscopy to measure the PL decay over time. Each data point correspondeds to a small wavelength increment. We then analyzed these datasets to determine the steady-state PL across a range of emission wavelengths at various times following excitation by a pulsed laser. Our objective is to examine and interpret the temporal trends in PL emission over time.

2.5 Photoluminescence Quantum Yield (PLQY)

Photoluminescence quantum yield measurements involve a quartz-tungsten-halogen lamp, an integrating sphere, a monochromator, and an IR detector. The inside of the integrating sphere has polytetrafluoroethylene (Teflon) coating, which helps to get uniform distribution of incident light inside the sphere. An 850 nm long pass filter and a 1000 nm short pass filter are placed at the entrance of the integrating sphere. The nanosheets dispersed in TCE are put in a quartz cuvette and mounted inside the integrating sphere for measurement. As shown in Figure 8[44], three separate measurements are required to calculate the QY. The first measurement is to find the intensity of light, off and on position measurements are with sample off and on the light beam pathway.

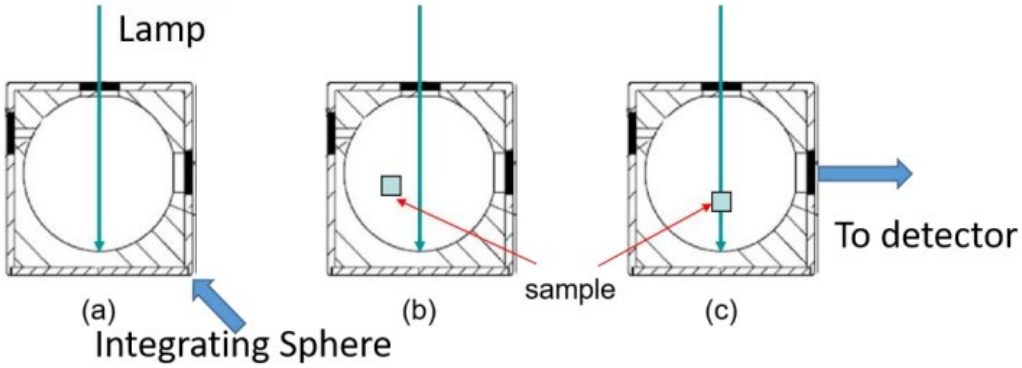

Figure 8. PLQY measurement using integrating sphere (a) measuring the intensity of light, (b) measuring the intensity when the sample is at off position from the light, (c) measuring the intensity when the sample is at on position from the light.

PLQY calculations are done following the procedure developed by Friend's group[45] as follows.

$$Quantum\ yield\ (\eta) = \frac{number\ of\ emitted\ photons}{number\ of\ absorbed\ photons}$$

$$Absorbance\ (A) = 1 - \frac{L_{0n}}{L_{off}}$$

$$\eta = \frac{P_{on} - (1 - A)P_{off}}{L_{lamp}A}$$

In these equations, A is the percentage of absorption, and L_{lamp}, L_{on}, and L_{off} are lamp spectrum intensities measurements a, c, and b, respectively. And P_{on} and P_{off} are lamp spectrum intensities multiplied by wavelengths of measurements b and c, corresponding to the number of photons.

2.6 X-Ray Diffraction (XRD)

The Bruker D8 XRD machine is used for XRD analysis. It is used to analyze the crystal structure of nanosheets and quantum dots. The sample was prepared by drop-casting the colloidal solution on a glass slab several times and letting it dry until an opaque thin film was formed. The thickness of nanosheets is estimated using the Scherrer equation below.

$$L = \frac{k\lambda}{\beta cos\theta}$$

In this equation, L is the thickness of the nanosheet, k = Scherrer constant, λ = X-ray wavelength, β = (full-width half maximum) FWHM of XRD peak, and θ = Bragg angle.

2.7 Transmission Electron Microscopy (TEM)

TEM works by directing an electron beam onto the sample, with the detector gathering the scattered electrons through the sample to produce an image at high resolution. This technique is used to verify the morphology of quantum dots and nanosheets. To prepare the sample for TEM, nanosheets or quantum dots diluted in TCA are drop cast on a special copper grid and allowed to dry for several minutes.

2.8 Thickness Measurement of Nanoribbons Using HRTEM Images

High-resolution transmission microscopy (HRTEM) images are used to measure the thickness of nanoribbons. Nanoribbons can stand on their side instead of lying flat on the surface

due to their smaller lateral dimensions. A free software, ImageJ, is used for measurement. We can use this software to measure the dimensions of any TEM images. First, a fixed scale is set on the software. Then we can draw a line across any part of the image and record the length. As the thickness of nanoribbons are not uniform, and the measurement is not precise, we need to take the data large enough to reduce the measurement errors and get an accurate average of the thickness.

2.9 Surface Passivation of Nanoribbons by Trioctylphosphine (TOP)

Surface passivation deactivates the surface trap states responsible for reducing the efficiency of the nanocrystals. Those trap states impair the mobility of charge carriers[46] and promote non-radiative recombination. To address these challenges, we passivate the PbS nanoribbons by TOP, where the phosphine of TOP is attached to bare Sulfur[47] on the surface, effectively neutralizing the trap site. The lead atoms on the surface are attached to oleic acid during growth and passivate themselves. Surface passivation suppresses the non-radiative decay, and enhances the photoluminescence decay lifetime, hence the quantum yield.

First, transfer the synthesized nanoribbons stored in toluene to passivate the sample to tetrachloroethylene (TCE) for passivation. Separate the nanoribbons from toluene by centrifuging or nitrogen dying process. Add one ml TCE and 0.1 ml TOP to the dried nanoribbons in the nitrogen environment. The container is filled with nitrogen gas, sealed using parafilm, and stored in a dark place.

CHAPTER 3. RESULTS AND DISCUSSIONS

3.1 TEM Images

Figure 9 shows TEM images of PbS nanoribbons synthesized at 70ºC. We can see the lateral dimensions are close to 20 nm wide. Nanoribbons can stand by their sides and form flower-like clusters, as in Figure 10(b).

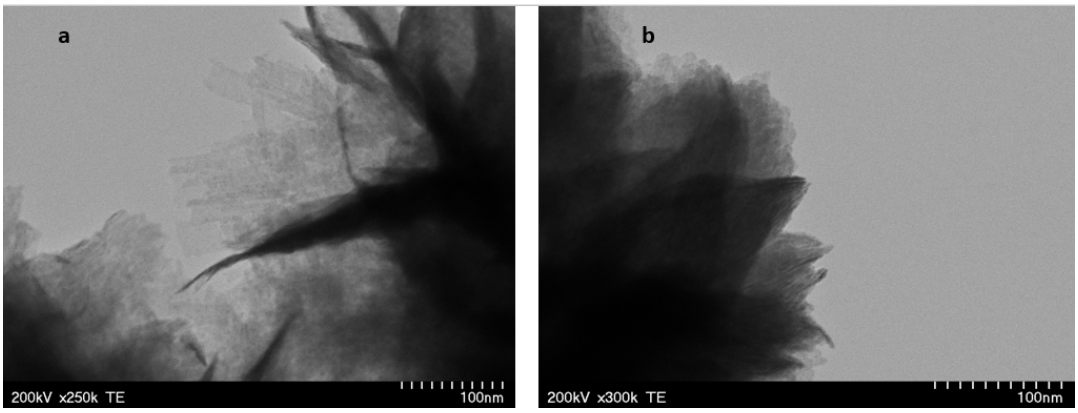

Figure 9. TEM images of nanoribbons synthesized at 70ºC (a) Nanoribbons with a width of about 20 nm, lying flat on the substrate (b) Nanoribbons stacked forming floral pattern indicating good crystallinity.

Figure 10 is the HRTEM of nanoribbons showing the side of it, where we can see arrays of atoms and count the stacks of the atomic layer in a nanoribbon. We can measure the thickness of nanoribbons and their interplanar spacing using this image.

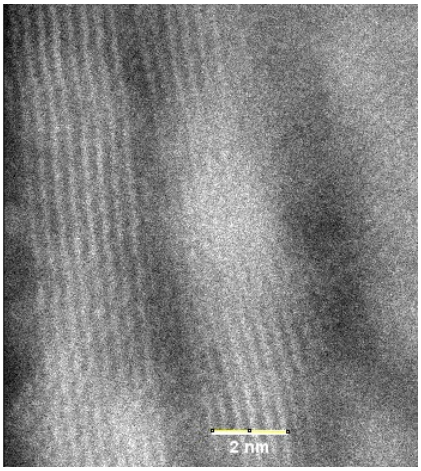

Figure 10. HRTEM image of PbS nanoribbons synthesized at 70ºC.

The thickness of PbS nanoribbons is measured using ImageJ software. This data is obtained through a rigorous process of conducting repetitive measurements of thicknesses using numbers of HRTEM images. All the measured data is plotted as a histogram in Figure 11.

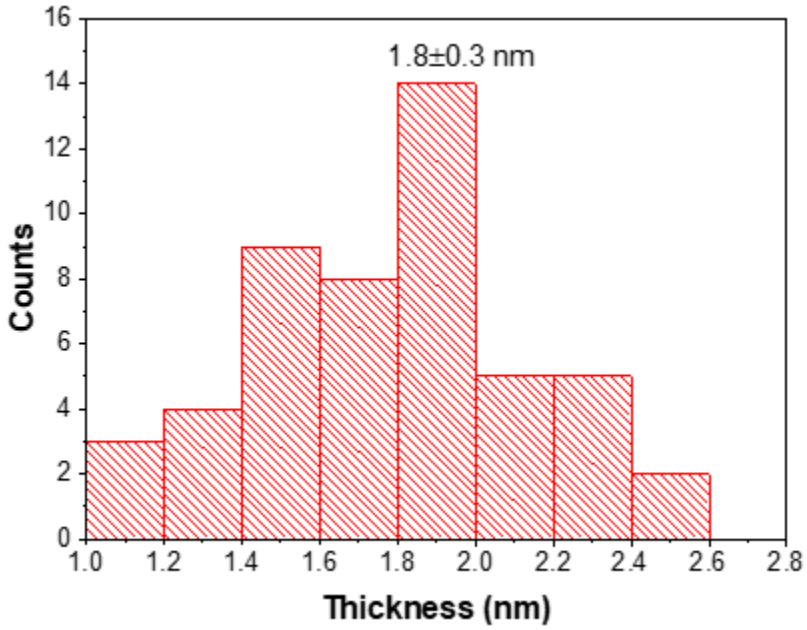

Figure 11. The histogram of the distribution of thicknesses of PbS nanoribbons synthesized at 70^0C, which were measured using ImageJ software. The average thickness is found to be 1.8 nm.

3.2 X-Ray Diffraction Measurement

The XRD results are used as the confirmatory indicators for the formation of PbS crystals in our synthesis. We can estimate the crystallite size of the nanoribbons from this measurement, which corresponds to the thickness of the nanoribbons. The thickness measured using this technique is not accurate because of the orientation of the crystal planes during the X-ray diffraction. Figure 12 shows the XRD measurements of PbS nanoribbons.

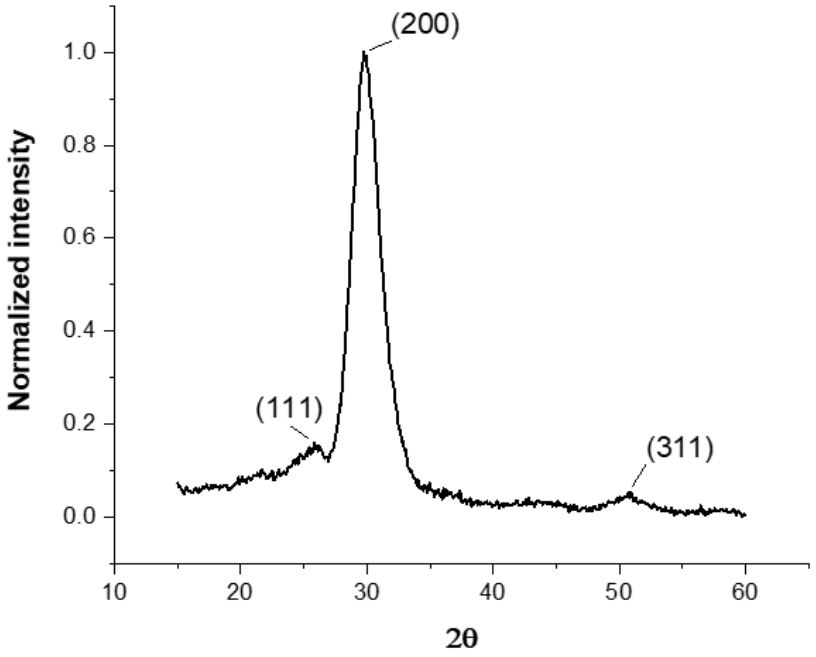

Figure 12. XRD spectrum of PbS nanoribbons synthesized at 70ºC.

We can see peaks corresponding to (111), (200), and (311) crystal planes of the PbS crystal structure. FWHM at 30º peak is used to calculate the crystallite size of PbS nanoribbons using the Scherrer equation. We have the equation to calculate the thickness (L):

$$L = \frac{k\lambda}{\beta cos\theta}$$

$$L = \frac{1 \times 0.15418}{\frac{5.23\pi}{180} \times \cos\left(\frac{29.99}{2}\right)}$$

$$L = 1.75\ nm$$

3.3 Photoluminescence Spectroscopy Measurements

Figure 13(a) shows the photoluminescence emission spectrum of original and TOP passivated PbS nanoribbons prepared at 70ºC, and Figure 13 (b) is an emission spectrum of PbS quantum dots synthesized at 90ºC. Quantum dots are brighter than nanosheets. TOP passivation can significantly enhance the emission of those nanosheets.

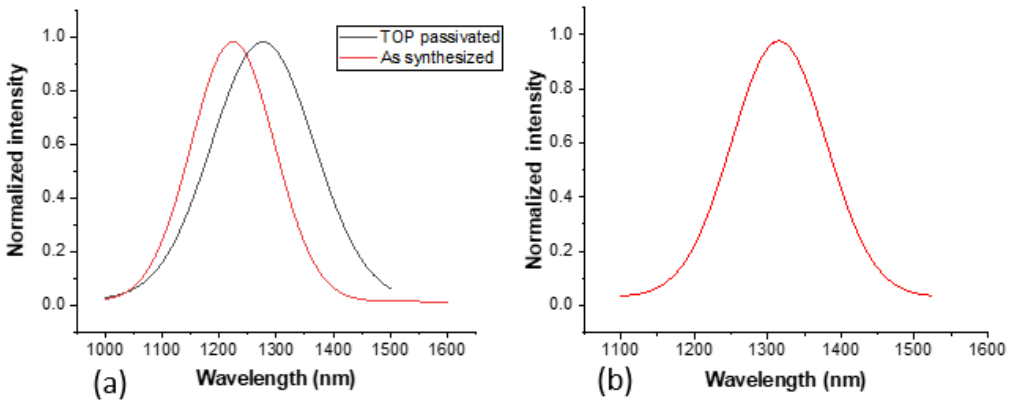

Figure 13. Photoluminescence spectrum of (a) PbS nanoribbons before and after TOP passivation, (b) PbS quantum dots.

The full-width half maxima (FWHM) of the emission spectrum are the characteristics of the sample's homogeneity. The photoluminescence spectrum becomes broader if the sample comprises a different thickness range. Our synthesis processes are refined over time to get homogeneous enough samples so that we do not have to separate the nanocrystals of varied sizes.

The photoluminescence spectrum also provides information about the thickness of most nanocrystals in the sample. The relation between the thickness and emission spectrum of PbS nanosheets and quantum dots is shown in Figure 14[35]. The energy gap of nanosheets decreases with an increase in their thickness. It is the consequence of the quantum confinement effect. Similarly, the energy gap decreases with the increase in the diameter of the quantum dot.

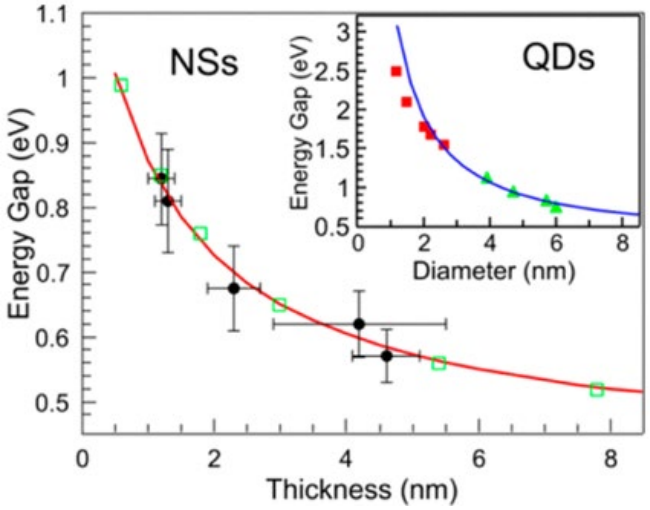

Figure 14. Relation between energy gaps (solid dots) and thickness of PbS nanosheets. Green squares are DFT-calculated data. Inset is the thickness dependence energy of quantum dots[35].

The thickness of nanosheets and the size of quantum dots are tuned by changing the reaction temperature. It shows the emissions of nanoribbons prepared at a temperature range 70ºC to 150ºC. We know the nanosheets prepared at higher temperatures are thicker than the nanosheets prepared at lower temperatures. Thinner nanosheets emit shorter wavelengths, and thicker ones emit longer wavelengths, as shown in Figure 15[44].

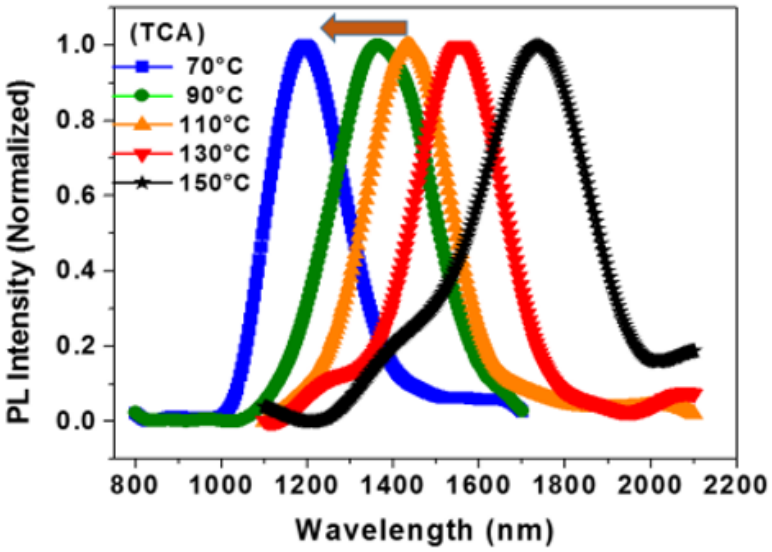

Figure 15: Photoluminescence spectrum of PbS nanoribbons synthesized at different temperatures from 70ºC to 150ºC.

In Figure 13(a), we can see that the spectrum is shifted towards the longer wavelength after TOP passivation. A similar phenomenon was reported in a study[48], that the dipoles of different ligands contract the crystal lattice causing the delocalization of electrons is partially responsible for the red shift in emission. Also, PbS nanosheets and quantum dots exhibit a blue shift in emission with time, known as the aging effect. Sometimes we can see the blue shift after TOP treatment as TOP is known to have an etching effect on PbS nanosheets, reducing the thickness, which explains the blue shift.

3.4 Photoluminescence Quantum Yield Measurements

Much research is going on to improve the quantum yield of semiconductor nanomaterials. It is crucial for efficient device applications. Understanding exciton dynamics in materials is essential to enhance quantum yield. A lot of work has been done on PbS quantum dots relating to their quantum yield efficiency and reported a range of improved efficiency up to 70%[49]. PbS quantum dots have a higher quantum yield than nanosheets. We have worked thoroughly on enhancing the photoluminescence quantum yield of PbS nanosheets in our group. Despite having a higher quantum yield, quantum dots have limitations for device applications. Therefore, enhancing the yield of nanosheets is in our interest.

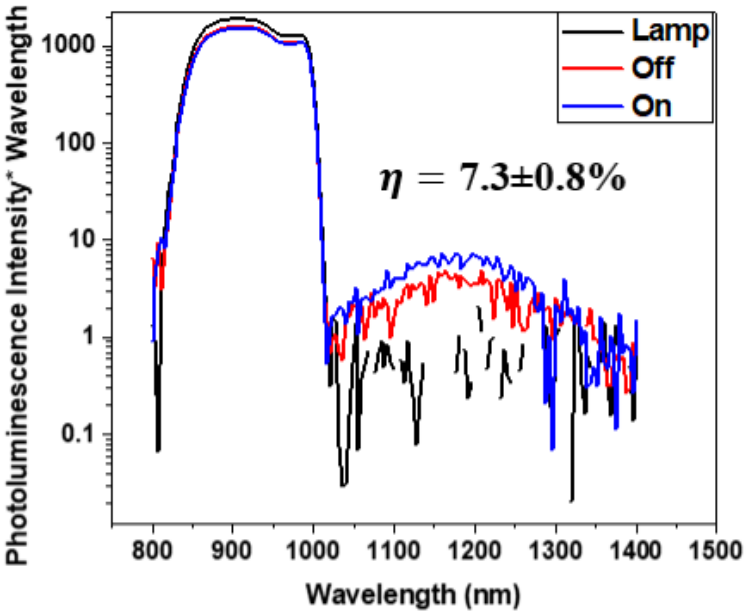

Figure 16. Absolute photoluminescence quantum yield measurement of PbS nanoribbons synthesized at 70°C. The quantum yield was found to be 7.3%.

We found the quantum yield of quantum dots to be around 20% and of nanoribbons less than 10%, as shown in Figure 16. The quantum yield of nanoribbons after passivating their surface using TOP improves the quantum yield to more than 26%[44]. Also, the quantum yield of quantum dots significantly drops when we measure them in their solid-state form. The decrease in quantum yield is due to the loss of surface ligand in solid state and activation of surface trap states facilitating the non-radiative recombination. On the other hand, the quantum yield of nanoribbons measured at solid state does not drop notably compared to quantum dots, as the nanosheet structure favors the densely packed ligands[32]. Therefore, nanoribbons are more advantageous than quantum dots for applicational purposes.

3.5 Time-Resolved Photoluminescence Measurements

Figure 17(a) shows the time-resolved photoluminescence decay spectrum of PbS nanoribbons before and after TOP passivation. There is a significant increase in photoluminescence lifetime after surface passivation. We find that, by deactivating the surface

defects, there is suppression in the non-radiative emission and enhanced efficiency of nanoribbons after TOP passivation. Also, nanoribbons exhibit double exponential photoluminescence decay, indicating surface trap states' significant presence. Figure 17 (b) is the photoluminescence decay of PbS quantum dots synthesized at 90°C. The decay trend is single exponential, which denotes fewer surface trap states on them.

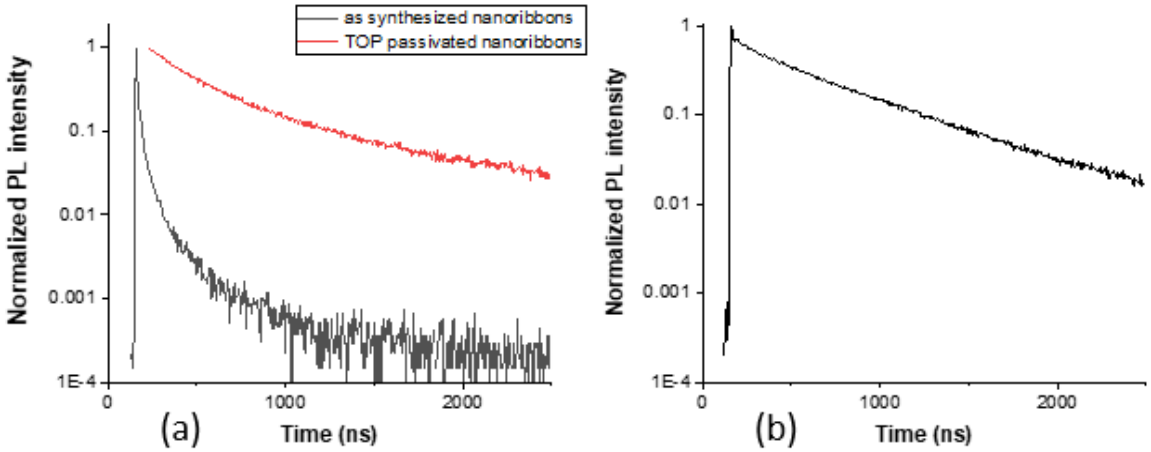

Figure 17. Time-resolved photoluminescence decay dynamics of (a) as-synthesized and TOP passivated PbS nanoribbons prepared at 70°C. (b) PbS quantum dots prepared at 90°C.

3.6 Time-Dependent Photoluminescence Spectrum

We plot the steady-state photoluminescence spectrum at various times after exciting the sample using a pulsed laser. Figure 18 shows the emission spectrum of PbS nanoribbons at various times. This data is obtained from the time-resolved PL spectrum measured at wavelengths over the emission spectrum of the nanoribbons. We measured the time-resolved photoluminescence decay using the TCSPC system. Each measurement is done in the interval of 3 nm, and the time at which the intensity is maximum is set as 0 ns. All the maximum intensities measured over the range of wavelength are plotted as photoluminescence spectrum at 0 ns. Similarly, the photoluminescence spectrum at various times in Figure 18 is plotted, extracting the data points from all the time-resolved photoluminescence decay measurements.

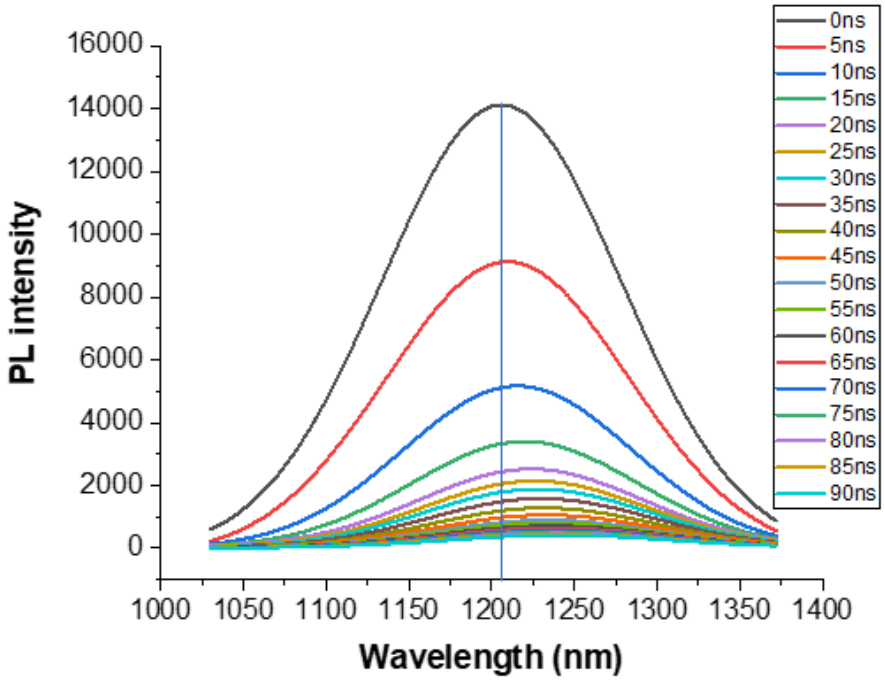

Figure 18. Time-dependent photoluminescence dynamics of as-synthesized PbS nanoribbons synthesized at 70°C.

As time progressed from zero ns to 90 ns, we observed a gradual red shift of the PL spectrum. Also, the emission intensity gradually decreases with time, which implies that delayed emission is not the dominating phenomenon. The redshift of the spectrum is due to the loss of energy during the process. The reason can be that the excited electrons experienced some anomaly costing time and energy before recombination.

The photoluminescence emission peak wavelength is plotted against the corresponding time to see the scale of the redshift. Figure 19 shows the trend of the shift in emission peak with time. There is a 40 nm redshift in emission peak in a 100 ns time interval.

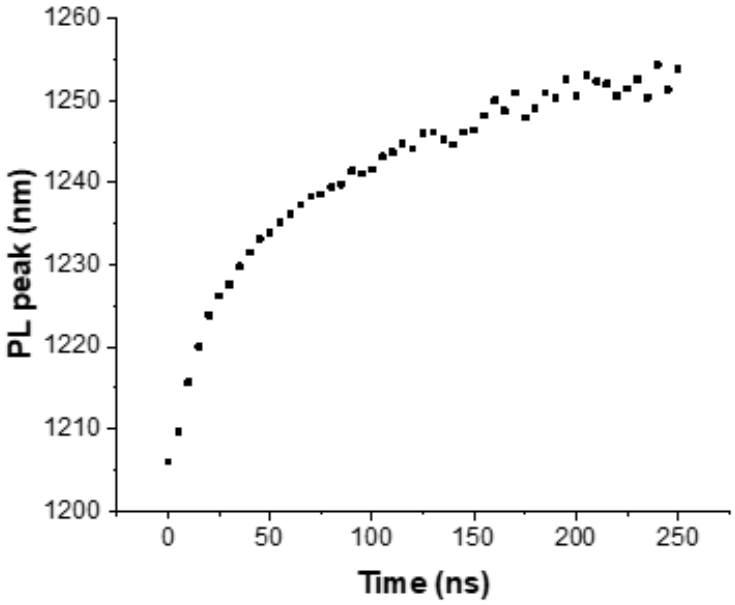

Figure 19. The photoluminescence peak emission wavelength of as-synthesized PbS nanoribbons at various times after excitation by a pulsed laser.

We suspect the redshift is due to the surface states and repeat the experiment using the surface passivated nanoribbons using TOP. Figure 20 is the static photoluminescence spectrum at various times after excitation for passivated nanoribbons. We can observe the spectral shift of surface passivated nanoribbons for a significantly longer time after excitation than the nanoribbons before passivation.

The increase in photoluminescence decay lifetime after TOP capping enhances the emission intensity later. The longer decay lifetime enables us to see the photoluminescence spectrum shift for a longer time. In Figure 19, we can see the emission intensity of nanoribbons before TOP passivation diminished significantly at 90 ns. However, the emission intensity of TOP passivated nanoribbons is quite large until hundreds of ns after excitation by the pulsed laser.

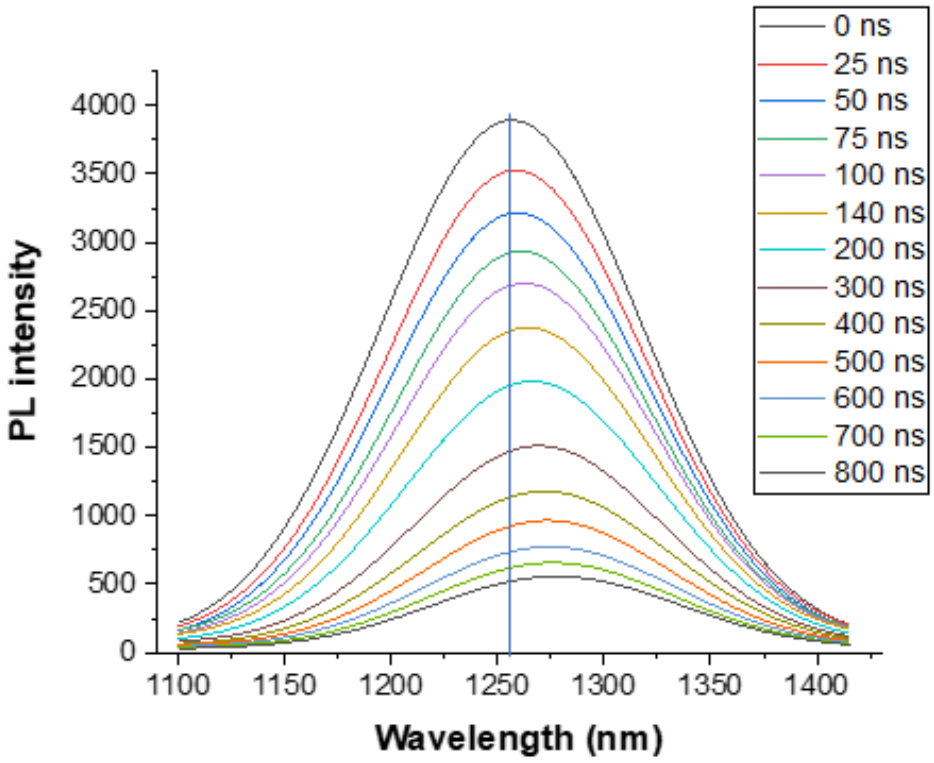

Figure 20. Time-dependent photoluminescence dynamics of TOP passivated PbS nanoribbons synthesized at 70°C.

Again, the photoluminescence emission peak wavelength of TOP-treated nanoribbons is plotted against the corresponding time to see the scale of the redshift. Figure 21 shows the shift in emission peak with time. There is a 25 nm redshift in emission peak in a 100 ns time interval. The trend is like the data of PbS nanoribbons before TOP treatment, but the time duration is significantly longer.

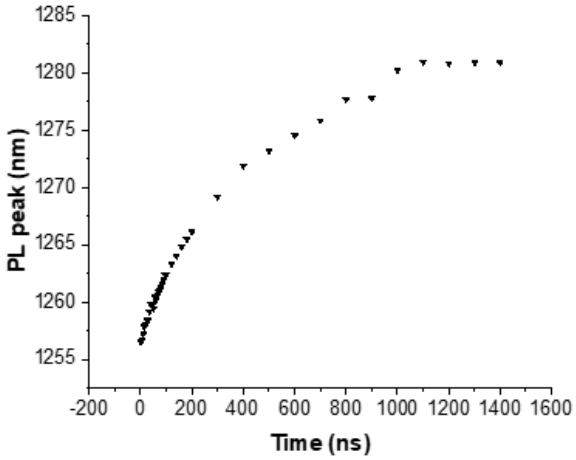

Figure 21. The photoluminescence peak emission wavelength of TOP passivated PbS nanoribbons at various times after excitation by a pulsed laser.

Comparing the emission shift of nanoribbons before and after TOP treatment, as shown in Figure 22, there is about a 40 nm shift in 100 ns and a 24 nm shift in 1000 ns, respectively. It is a substantial decrease in redshift with time. The suppression in the red shift in passivated nanoribbons signals surface defects is the reason for the redshift. The excited electrons might have been trapped in the surface states due to defects, delaying relaxation and losing some energy in the process before recombination.

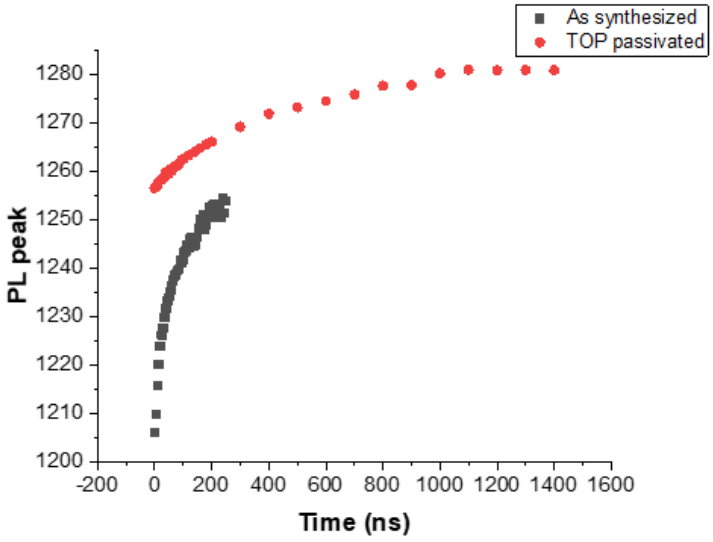

Figure 22. Comparison of photoluminescence peak shift of as-synthesized and TOP passivated PbS nanoribbons.

To confirm the contributions of trap states for the red shift in the emission spectrum, we did the control experiment with the specimen having a significantly lower number of surface defects. PbS quantum dots have a much lesser number of surface defects than nanosheets, which is confirmed by their photoluminescence decay lifetime and higher quantum. So, we repeat the experiment with PbS quantum dots, and the resulting time-dependent photoluminescence spectrum is shown in Figure 23.

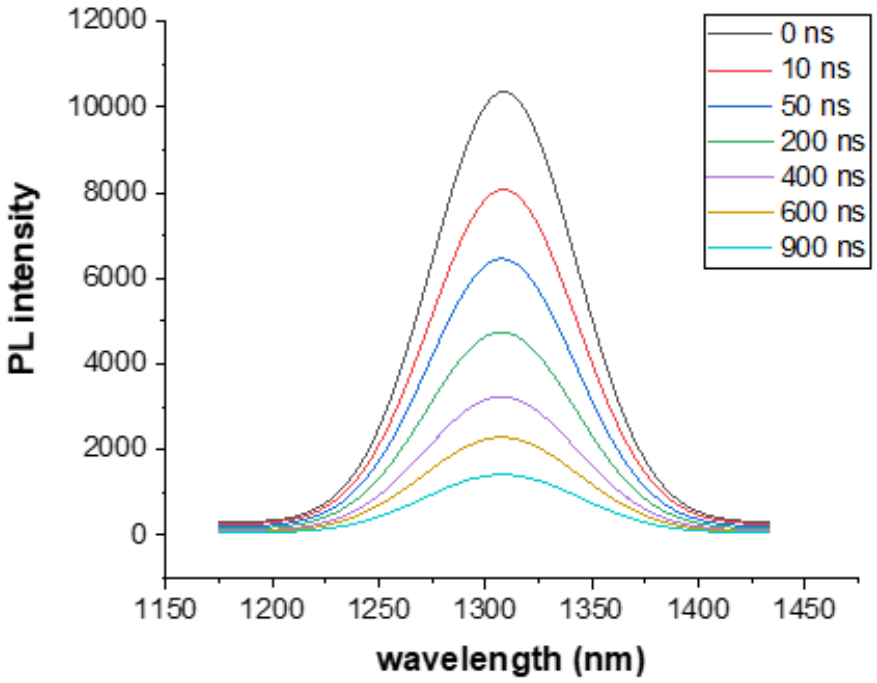

Figure 23. Time-dependent photoluminescence dynamics of PbS quantum dots synthesized at 90ºC.

The longer photoluminescence lifetime of PbS quantum dots allows us to see the static photoluminescence spectrum of a few hundred nanoseconds time after excitation. The delayed emissions from PbS quantum dots do not show any redshift this time. Since the quantum dots have very few surface states compared to nanoribbons, we can confirm that the presence of trap states on the surfaces of nanoribbons contributes to the redshift on delayed photoluminescence emission.

3.6.1 Discussions

We confirmed that surface defects play a role in the redshift of the photoluminescence spectrum at later times after excitation. Electrons excited by absorbing photons are trapped in the surface states while diffusing in the conduction band, as shown in Figure 24. The higher defect density prevents the excitons from diffusing further away and traps them into those surface states, which explains the low photoluminescence decay lifetime of the original nanoribbons. After surface passivation, excited electrons can diffuse in the conduction band further away, increasing the photoluminescence lifetime.

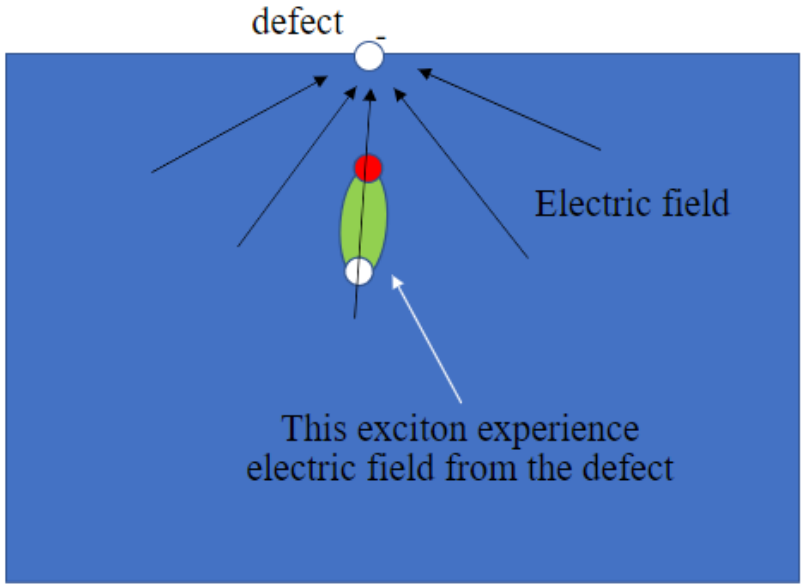

Figure 24. Excitons trapped in surface defects of nanoribbons before TOP passivation.

The energy loss is due to the excited electrons experiencing the instantaneously formed energy states by the interference of trap states and regular energy states. Any quantum-confined system exposed to an electric field along the confinement direction gives rise to the quantum-confined Stark effect (QCSE)[50]. As-synthesized nanoribbons have a larger number of surface defects which can induce a certain electric field, resulting in the Stark effect. The Stark effect shifts the energy level of holes and electrons, decreasing their energy gap[51-53]. Which

consequently shifts the photoluminescence emission to the lower energy, causing the speculated redshift. There are fewer defects after TOP passivation, as shown in Figure 25, decreasing the defects-induced electric field, which will eventually lower the Stark effect, eliminating the redshift.

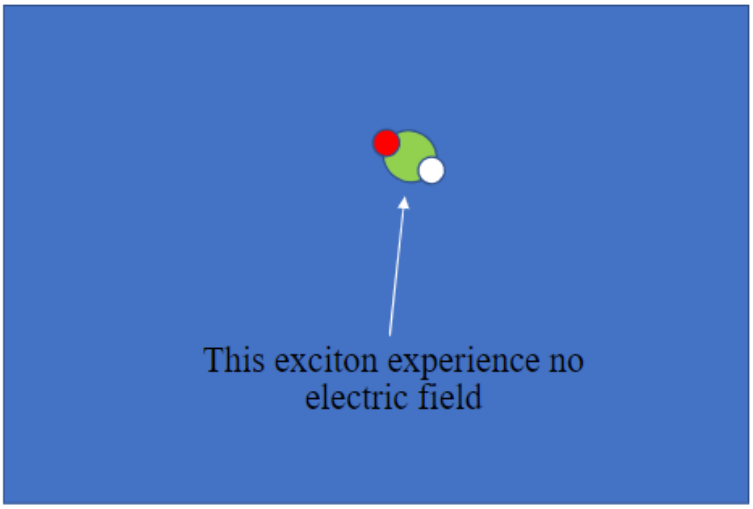

Figure 25. Excitons do not get trapped in defects of nanoribbon after TOP passivation, as there are reduced numbers of defects affecting fewer excitons.

On the other hand, quantum dots are tiny compared to nanosheets; as shown in Figure 26, they cannot generate multiple excitons. The single exciton is not strong enough to screen the Stark effect caused by the surface defects. Also, quantum dots have fewer defects at different orientations compared to nanoribbons and thus cannot generate a notable Stark effect. Therefore, there is no redshift in the time-dependent photoluminescence spectrum of PbS quantum dots. This verifies that the surface defects in nanoribbons are the cause of the redshift in the time-dependent photoluminescence spectrum.

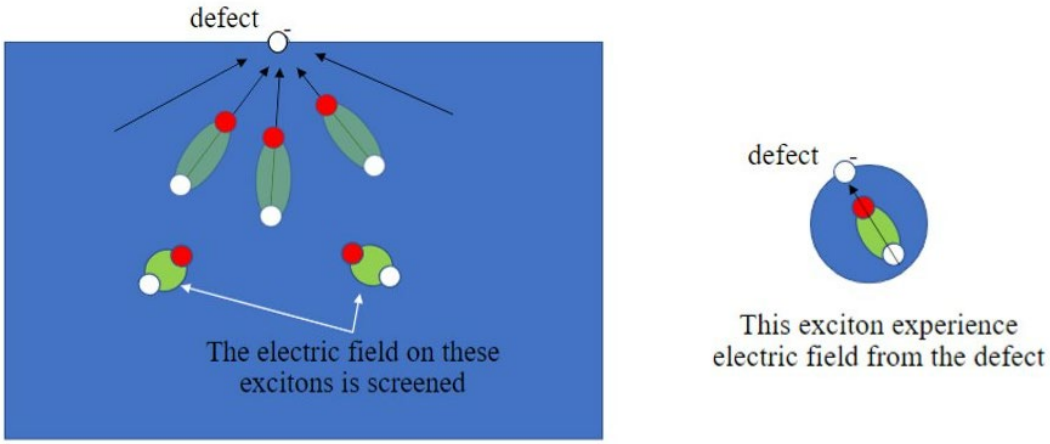

Figure 26. Excitons in nanoribbon compared to quantum dot after excitation by a pulsed laser, indicating not enough excitons in quantum dot to screen the Stark effect.

3.7 Effects of Excitation Power on Photoluminescence Spectrum

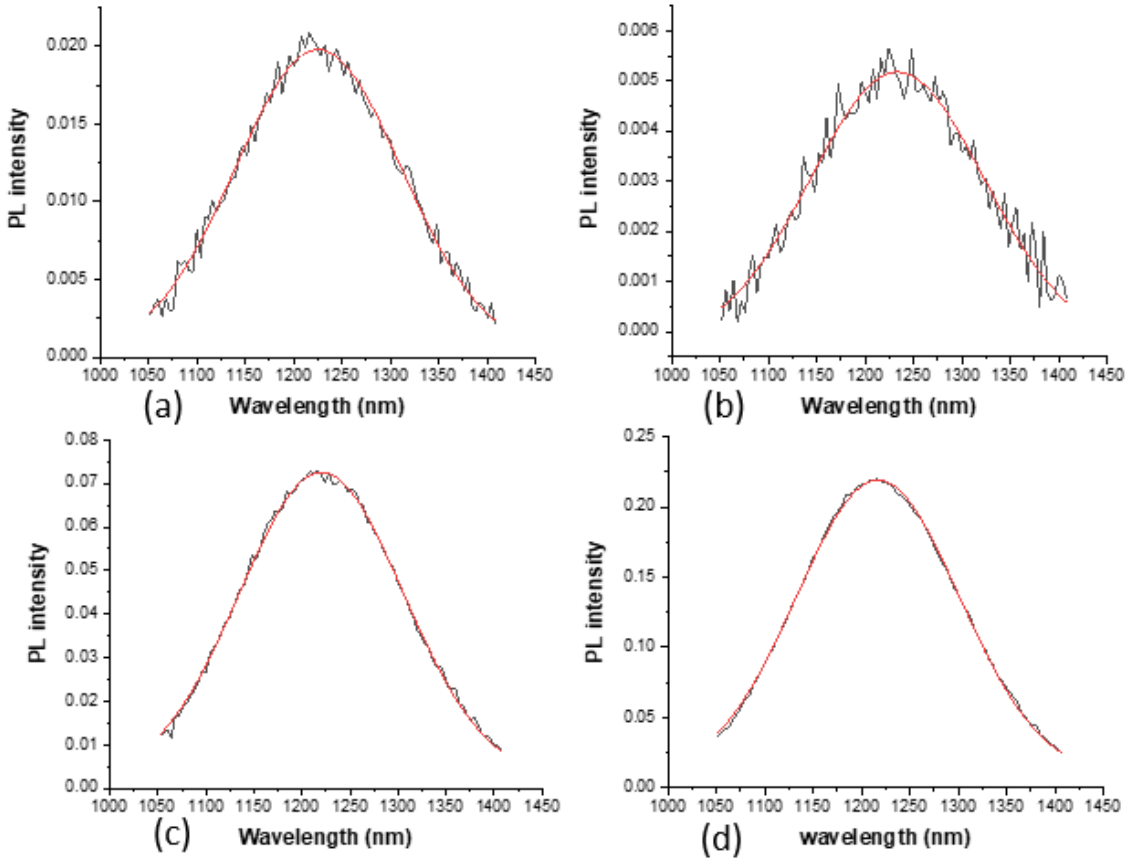

Figure 27. Photoluminescence spectrum of PbS nanoribbons by exciting sample by laser power (a) 0.1 milliwatts, (b) 0.4 milliwatts, (c) 1.6 milliwatts, and (d) 6.4 milliwatts.

We studied the effect of excitation power on static and time-resolved photoluminescence. Figure 27 shows the static photoluminescence spectrum from PbS nanoribbons at excitation laser power from 0.1 milliwatts (mW) to 6.4 milliwatts. The intensity of emission increases with an increase in excitation power, but the emission spectrum is shifted towards the higher energy. The photoluminescence peaks shift towards shorter wavelengths with an increase in excitation laser power. Emission peaks at different excitation powers are shown in Table 1.

Table 1. The photoluminescence emission peak of PbS nanoribbons at different pumping power. The emission peak shifted towards a shorter wavelengths with an increase in laser power.

Laser power (mW)	PL peak (nm)
0.1	1233
0.4	1225
1.6	1220
6.4	1217

The photoluminescence peak is at 1233 nm when the excitation laser power was 0.1 mW and decreases to 1217 nm when the laser power increased to 6.4 mW. This shift in emission spectrum could be raised due to an increased number of excited electrons, or it may occur by the degradation of nanoribbons by continuous exposure to the laser beam.

To see the effect of the laser on the nanoribbons, we exposed the sample to the laser power of up to 9 mW for 4 minutes, which is more than the duration of our regular photoluminescence spectrum measurement. We recorded the static emission at a fixed wavelength of 1220 nm and measured the emission intensity over time. There was a negligible fluctuation in the emission intensity, as shown in Figure 28. Therefore, we ruled out that the degradation of the sample by the laser causes the blueshift.

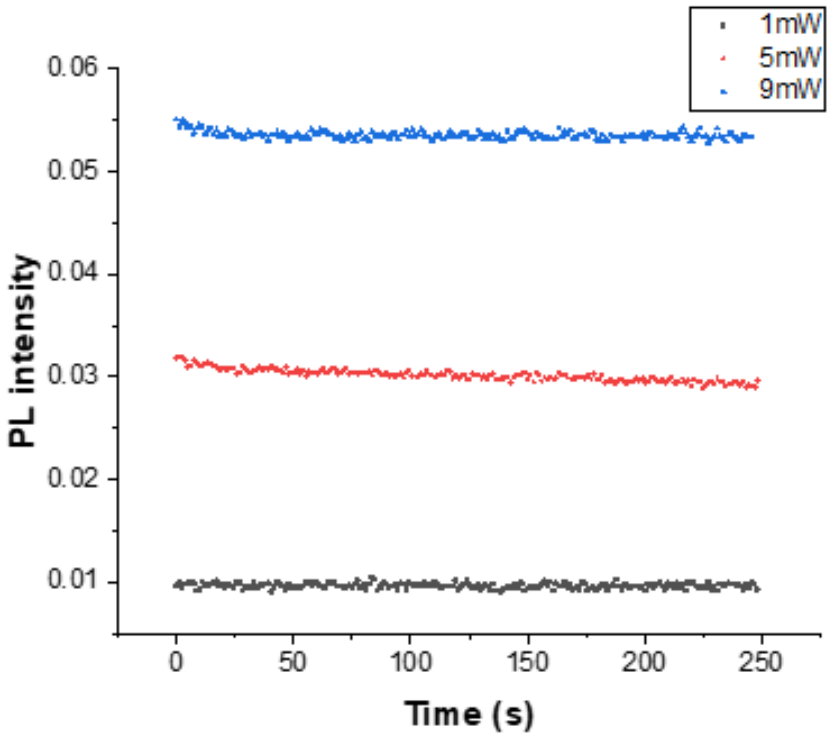

Figure 28. Static photoluminescence spectrum of PbS nanoribbons at measure at 1220 nm wavelength using 200-kilohertz pulsed laser of wavelength 532 nm.

Next, we measured the photoluminescence decay of PbS nanoribbons with the excitation laser power ranging from 0.5 mW to 20 mW. Figure 29 shows the photoluminescence decay of excitons generated using the pulsed laser of various intensities. The photoluminescence decay rate is faster with an increase in excitation laser power. Therefore, blueshift in the static photoluminescence spectrum and the decrease in decay lifetime with an increase in excitation laser power should be related.

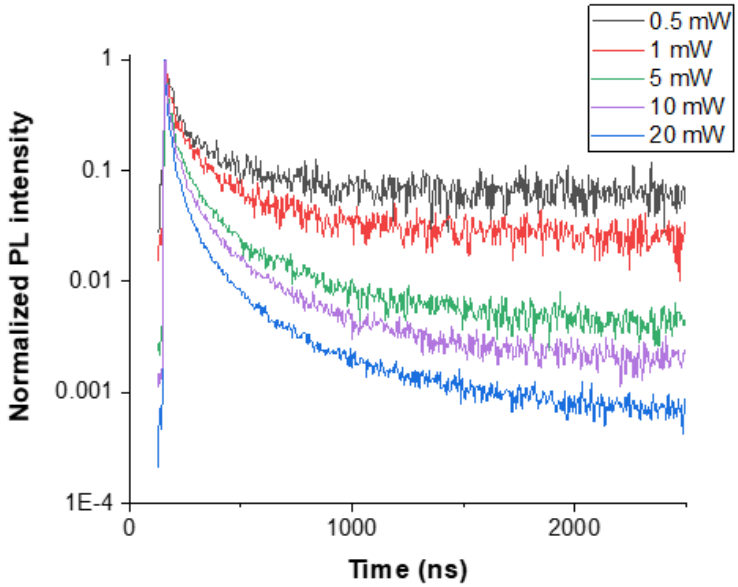

Figure 29. Time-resolved photoluminescence spectrum of PbS nanoribbons at different excitation intensities.

The photoluminescence decay lifetime is estimated from the decay spectrum in Figure 29. The decay lifetime is the time taken by the numbers of originally photoexcited electrons to decrease by factor 1/e or 37%. The e-fold decay lifetime decreasing from maximum intensity to 37% is shown in Table 2. The decay lifetime decreases from 44 ns to 13 ns when excited by laser power from 0.5 mW to 20 mW, respectively.

Table 2. Photoluminescence decay 1/e lifetimes of PbS nanoribbons at different pumping power. The decay lifetimes showed a decreasing trend with an increase in laser power.

Laser power (mW)	Lifetime (ns)
0.5	44
1	38
5	18
10	16
20	13

3.7.1 Discussions

The change in static and time-resolved photoluminescence spectrum behavior results from the building of charge carriers on the conduction band with increased excitation laser power. Reale et al.[54] report and explain the spectral shift with increased excitation power. The shift is due to more vigorous screening of the built-in electric field at increasing excitation power[54]. The same effect is responsible for the decrease in photoluminescence decay lifetime. The excited states are strongly screened by the electric field build-up by the excited electrons when using higher pumping power, forcing the excited electrons to recombine faster. Therefore, higher pumping power creates a stronger electric field which screens the excited states, decreasing the decay time.

3.8 Conclusions

Surface defects in nanosheets or nanoribbons can significantly affect their optical properties and behavior. Surface defects introduce an electric field that influences the energy levels of the nanosheets through a phenomenon called the Stark effect. The Stark effect refers to shifting energy levels in response to an external electric field. This effect causes a redshift in the static photoluminescence spectrum. To mitigate the impact of surface defects and counteract the redshift in the photoluminescence spectrum, the nanosheets and nanoribbons are treated with a surface ligand which helps eliminate or reduce the surface states and subsequently reduces the Stark effect, suppressing the redshift in the PL spectrum. Quantum dots, which have relatively defect-free surfaces, do not exhibit a redshifted photoluminescence emission and exhibit more stable and consistent emission properties than nanosheets.

In a subsequent experiment on nanoribbons before surface passivation, the photoluminescence spectrum displays a blue shift as the excitation laser power increases. This

observation suggests that with increasing excitation power, the electric field generated by more excited electrons becomes stronger, effectively screening out the Stark effect. This screening allows the nanoribbons to establish their original energy gap (no Stark effect).

The Stark effect arises from the interaction between the electric field and the electric dipole moment. The excitons can induce dipole moments around themselves, and any external electric field interacts with the dipole and causes the Stark effect. The recombination dynamics of excitons are affected by the Stark effect. The recombination rates depend on several factors, such as overlap between the electron and hole wavefunction, the density of states, and the selection rule governing the emission process. When an external field is applied, it alters the electron and hole wavefunctions due to the splitting and shifting of energy levels called Stark-shifted states. If the Stark effect reduces the overlap of electron and hole wavefunction, it decreases the radiative recombination rate. Higher excitation power excites a higher number of electrons, which reduces the Stark effect, enhancing the recombination rate. The accurate impact of the Stark effect on the recombination rate depends on the strength and direction of the electric field induced by the surface defects. Therefore, the defect density plays a vital role in the recombination dynamics of excitons.

These findings highlight the importance of understanding and controlling surface defects in nanomaterials, as they can significantly influence their optical properties, energy levels, and emission characteristics. Besides the Stark effect caused by the surface defects, there are other crucial factors that can affect the behavior of excitons, such as exciton-exciton interaction and Auger recombination. Our next step is evaluating the existence of these elements and their influence on the efficiency of nanomaterials so that we can enhance the efficiency of nanoscale optoelectronic devices and explore their potential applications in various fields.

REFERENCES

1. Pandey, P., Role of nanotechnology in electronics: A review of recent developments and patents. *Recent Patents on Nanotechnology* **2022,** *16* (1), 45-66.

2. Korkin, A.; Gusev, E.; Labanowski, J. K.; Luryi, S., *Nanotechnology for electronic materials and devices*. Springer Science & Business Media: 2010.

3. Contera, S.; Bernardino de la Serna, J.; Tetley, T. D., Biotechnology, nanotechnology and medicine. *Emerging Topics in Life Sciences* **2020,** *4* (6), 551-554.

4. Surendiran, A.; Sandhiya, S.; Pradhan, S.; Adithan, C., Novel applications of nanotechnology in medicine. *Indian Journal of Medical Research* **2009,** *130* (6), 689-701.

5. Wang, C.; Irudayaraj, J., Gold nanorod probes for the detection of multiple pathogens. *small* **2008,** *4* (12), 2204-2208.

6. Xu, X.; Ying, Y.; Li, Y., Gold nanorods based LSPR biosensor for label-free detection of alpha-fetoprotein. *Procedia Engineering* **2011,** *25*, 67-70.

7. Ali Mansoori, G.; Bastami, T. R.; Ahmadpour, A.; Eshaghi, Z., Environmental application of nanotechnology. *Annual review of nano research* **2008**, 439-493.

8. Guerra, F. D.; Attia, M. F.; Whitehead, D. C.; Alexis, F., Nanotechnology for environmental remediation: materials and applications. *Molecules* **2018,** *23* (7), 1760.

9. Cheng, H. N.; Klasson, K.; Asakura, T.; Wu, Q., Nanotechnology in agriculture. In *Nanotechnology: Delivering on the Promise Volume 2*, ACS Publications: 2016; pp 233-242.

10. Usman, M.; Farooq, M.; Wakeel, A.; Nawaz, A.; Cheema, S. A.; ur Rehman, H.; Ashraf, I.; Sanaullah, M., Nanotechnology in agriculture: Current status, challenges and future opportunities. *Science of the Total Environment* **2020,** *721*, 137778.

11. Asha, A. B.; Narain, R., Nanomaterials properties. In *Polymer science and nanotechnology*, Elsevier: 2020; pp 343-359.

12. Ramalingam, G.; Kathirgamanathan, P.; Ravi, G.; Elangovan, T.; Manivannan, N.; Kasinathan, K., Quantum confinement effect of 2D nanomaterials. In *Quantum Dots-Fundamental and Applications*, IntechOpen: 2020.

13. Schaefer, H.-E., *Nanoscience: the science of the small in physics, engineering, chemistry, biology and medicine*. Springer Science & Business Media: 2010.

14. Kittel, C., *Introduction to solid state physics*. John Wiley & sons, inc: 2005.

15. Myasnikov, E.; Myasnikova, A., Band theory of semiconductors and autolocalization of electrons. *Physics Letters A* **2001,** *286* (2-3), 210-216.

16. Machol, J.; Wise, F.; Patel, R.; Tanner, D., Optical studies of IV–VI quantum dots. *Physica A: Statistical Mechanics and its Applications* **1994,** *207* (1-3), 427-434.

17. Schmid, G., *Nanoparticles: from theory to application*. John Wiley & Sons: 2011.

18. Itoh, T.; Ikehara, T.; Iwabuchi, Y., Quantum confinement of excitons and their relaxation processes in CuCl microcrystals. *Journal of luminescence* **1990,** *45* (1-6), 29-33.

19. Zhu, K.; Shi, J.; Zhang, L., Preparation and optical absorption of InSb microcrystallites embedded in SiO2 thin films. *Solid state communications* **1998,** *107* (2), 79-84.

20. Konstantatos, G.; Sargent, E. H., *Colloidal quantum dot optoelectronics and photovoltaics*. Cambridge University Press: 2013.

21. Wise, F. W., Lead salt quantum dots: the limit of strong quantum confinement. *Accounts of Chemical Research* **2000,** *33* (11), 773-780.

22. Katan, C.; Mercier, N.; Even, J., Quantum and Dielectric Confinement Effects in Lower-Dimensional Hybrid Perovskite Semiconductors. *Chemical Reviews* **2019,** *119* (5), 3140-3192.

23. Norris, D. J. Measurement and assignment of the size-dependent optical spectrum in cadmium selenide (CdSe) quantum dots. Massachusetts Institute of Technology, 1995.

24. Reiss, P., *Synthesis of semiconductor nanocrystals in organic solvents*. Springer: 2008.

25. Harris, D. K. Synthesis and characterization of infrared quantum dots. Massachusetts Institute of Technology, 2014.

26. Hines, M. A.; Scholes, G. D., Colloidal PbS nanocrystals with size-tunable near-infrared emission: observation of post-synthesis self-narrowing of the particle size distribution. *Advanced Materials* **2003,** *15* (21), 1844-1849.

27. Cademartiri, L.; Montanari, E.; Calestani, G.; Migliori, A.; Guagliardi, A.; Ozin, G. A., Size-dependent extinction coefficients of PbS quantum dots. *Journal of the American Chemical Society* **2006,** *128* (31), 10337-10346.

28. Choi, H.; Ko, J.-H.; Kim, Y.-H.; Jeong, S., Steric-hindrance-driven shape transition in PbS quantum dots: understanding size-dependent stability. *Journal of the American Chemical Society* **2013,** *135* (14), 5278-5281.

29. Qian, G.; Zhong, Z.; Luo, M.; Yu, D.; Zhang, Z.; Wang, Z. Y.; Ma, D., Simple and efficient near-infrared organic chromophores for light-emitting diodes with single electroluminescent emission above 1000 nm. *Advanced Materials* **2009,** *21* (1), 111-116.

30. Semonin, O. E.; Johnson, J. C.; Luther, J. M.; Midgett, A. G.; Nozik, A. J.; Beard, M. C., Absolute photoluminescence quantum yields of IR-26 dye, PbS, and PbSe quantum dots. *The journal of physical chemistry letters* **2010,** *1* (16), 2445-2450.

31. Sommer, J. R.; Farley, R. T.; Graham, K. R.; Yang, Y.; Reynolds, J. R.; Xue, J.; Schanze, K. S., Efficient near-infrared polymer and organic light-emitting diodes based on electrophosphorescence from (tetraphenyltetranaphtho [2, 3] porphyrin) platinum (II). *ACS applied materials & interfaces* **2009,** *1* (2), 274-278.

32. Schliehe, C.; Juarez, B. H.; Pelletier, M.; Jander, S.; Greshnykh, D.; Nagel, M.; Meyer, A.; Foerster, S.; Kornowski, A.; Klinke, C., Ultrathin PbS sheets by two-dimensional oriented attachment. *Science* **2010,** *329* (5991), 550-553.

33. Tang, Y., *Exciton Physics of Colloidal Nanostructures and Metal Oxides*. Bowling Green State University: 2021.

34. áPeter Lu, H., Growth of colloidal PbS nanosheets and the enhancement of their photoluminescence. *Physical Chemistry Chemical Physics* **2015,** *17* (36), 23303-23307.

35. Bhandari, G. B.; Subedi, K.; He, Y.; Jiang, Z.; Leopold, M.; Reilly, N.; Lu, H. P.; Zayak, A. T.; Sun, L., Thickness-controlled synthesis of colloidal PbS nanosheets and their thickness-dependent energy gaps. *Chemistry of Materials* **2014,** *26* (19), 5433-5436.

36. Premathilaka, S. M.; Jiang, Z.; Antu, A.; Leffler, J.; Hu, J.; Roy, A.; Sun, L., A robust method for the synthesis of colloidal PbS nanosheets. *physica status solidi (RRL)–Rapid Research Letters* **2016,** *10* (11), 838-842.

37. Zhang, H.; Savitzky, B. H.; Yang, J.; Newman, J. T.; Perez, K. A.; Hyun, B.-R.; Kourkoutis, L. F.; Hanrath, T.; Wise, F. W., Colloidal synthesis of PbS and PbS/CdS nanosheets using acetate-free precursors. *Chemistry of Materials* **2016,** *28* (1), 127-134.

38. Bielewicz, T.; Ramin Moayed, M. M.; Lebedeva, V.; Strelow, C.; Rieckmann, A.; Klinke, C., From dots to stripes to sheets: shape control of lead sulfide nanostructures. *Chemistry of Materials* **2015,** *27* (24), 8248-8254.

39. Antu, A. D.; Jiang, Z.; Premathilka, S. M.; Tang, Y.; Hu, J.; Roy, A.; Sun, L., Bright colloidal PbS nanoribbons. *Chemistry of Materials* **2018,** *30* (11), 3697-3703.

40. Khan, A. H.; Brescia, R.; Polovitsyn, A.; Angeloni, I.; Martín-García, B.; Moreels, I., Near-Infrared emitting colloidal PbS nanoplatelets: lateral size control and optical spectroscopy. *Chemistry of Materials* **2017,** *29* (7), 2883-2889.

41. Millar, S., Tips and Tricks for the Lab: Air-Sensitive Techniques (1). *ChemViews* **2013**.

42. Hwang, G. Surface trap passivation and characterization of lead sulfide quantum dots for optical and electrical applications. Massachusetts Institute of Technology, 2015.

43. Critchley, L. What is the Difference Between Fluorescence and Phosphorescence? https://www.azooptics.com/Article.aspx?ArticleID=1326 (accessed June 16, 2023).

44. Antu, A. D. Morphology and surface passivation of colloidal PbS nanoribbons. Bowling Green State University, 2017.

45. de Mello, J. C.; Wittmann, H. F.; Friend, R. H., An improved experimental determination of external photoluminescence quantum efficiency. *Advanced materials* **1997,** *9* (3), 230-232.

46. Jeong, K. S.; Tang, J.; Liu, H.; Kim, J.; Schaefer, A. W.; Kemp, K.; Levina, L.; Wang, X.; Hoogland, S.; Debnath, R., Enhanced mobility-lifetime products in PbS colloidal quantum dot photovoltaics. *ACS nano* **2012,** *6* (1), 89-99.

47. Tang, J.; Kemp, K. W.; Hoogland, S.; Jeong, K. S.; Liu, H.; Levina, L.; Furukawa, M.; Wang, X.; Debnath, R.; Cha, D., Colloidal-quantum-dot photovoltaics using atomic-ligand passivation. *Nature materials* **2011,** *10* (10), 765-771.

48. Diroll, B. T., Ligand-Dependent Tuning of Interband and Intersubband Transitions of Colloidal CdSe Nanoplatelets. *Chemistry of Materials* **2020,** *32* (13), 5916-5923.

49. Greben, M.; Fucikova, A.; Valenta, J., Photoluminescence quantum yield of PbS nanocrystals in colloidal suspensions. *Journal of Applied Physics* **2015,** *117* (14), 144306.

50. Walters, G.; Wei, M.; Voznyy, O.; Quintero-Bermudez, R.; Kiani, A.; Smilgies, D.-M.; Munir, R.; Amassian, A.; Hoogland, S.; Sargent, E., The quantum-confined Stark effect in layered hybrid perovskites mediated by orientational polarizability of confined dipoles. *Nature communications* **2018,** *9* (1), 4214.

51. Schmitt-Rink, S.; Chemla, D.; Miller, D. A., Linear and nonlinear optical properties of semiconductor quantum wells. *Advances in Physics* **1989,** *38* (2), 89-188.

52. Miller, D. A.; Chemla, D.; Damen, T.; Gossard, A.; Wiegmann, W.; Wood, T.; Burrus, C., Electric field dependence of optical absorption near the band gap of quantum-well structures. *Physical Review B* **1985,** *32* (2), 1043.

53. Miller, D. A.; Chemla, D.; Damen, T.; Gossard, A.; Wiegmann, W.; Wood, T.; Burrus, C., Band-edge electroabsorption in quantum well structures: The quantum-confined Stark effect. *Physical Review Letters* **1984,** *53* (22), 2173.

54. Reale, A.; Massari, G.; Di Carlo, A.; Lugli, P.; Vinattieri, A.; Alderighi, D.; Colocci, M.; Semond, F.; Grandjean, N.; Massies, J., Comprehensive description of the dynamical screening of the internal electric fields of AlGaN/GaN quantum wells in time-

resolved photoluminescence experiments. *Journal of applied physics* **2003,** *93* (1), 400-409.